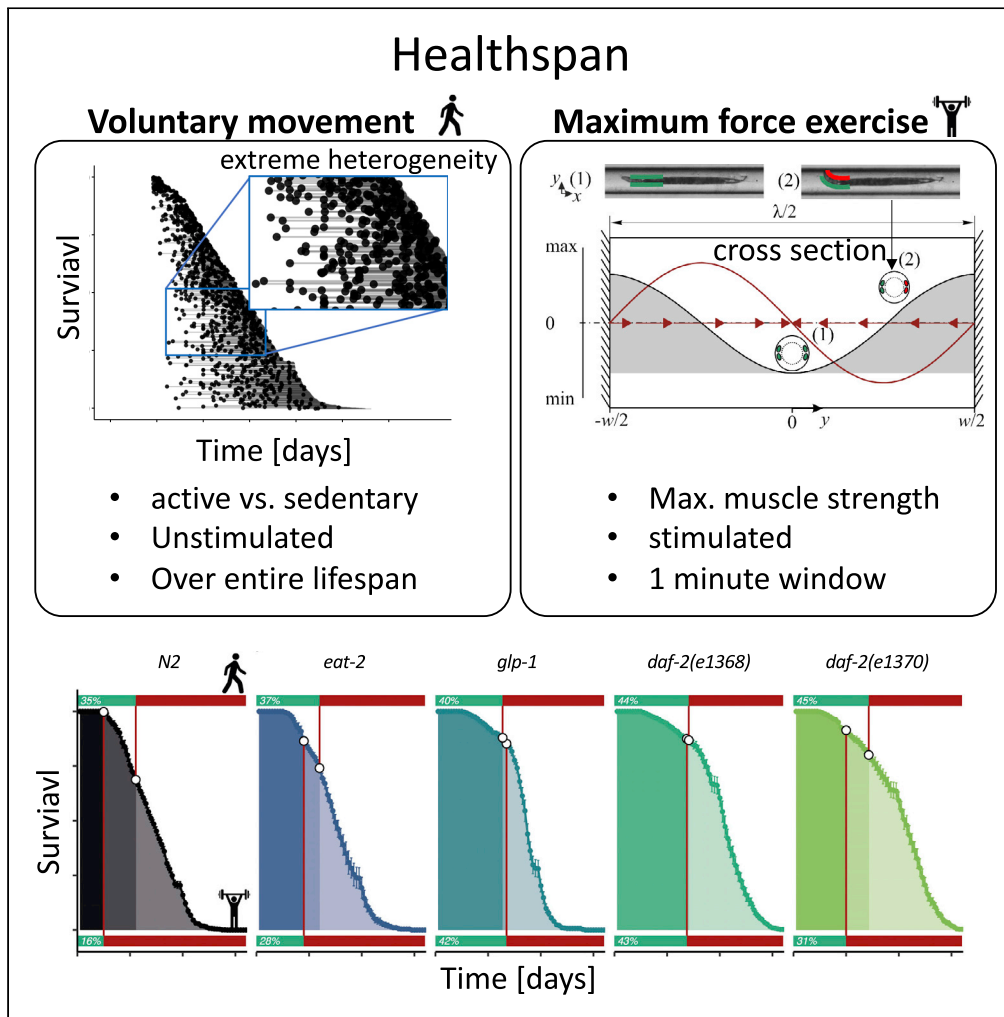**Article**

Longevity interventions temporally scale healthspan in *Caenorhabditis elegans*

Cyril Statzer, Peter Reichert, Jürg Dual, Collin Y. Ewald

collin-ewald@ethz.ch (C.Y.E.)
dual@imes.mavt.ethz.ch (J.D.)

Highlights

We developed a microfluidics device to assess healthspan of *C. elegans*

Acoustophoretic force fields to quantify dynamic muscle power

Healthspan is neither extended nor compressed by longevity interventions

Article

Longevity interventions temporally scale healthspan in *Caenorhabditis elegans*

Cyril Statzer,[1,3] Peter Reichert,[2,3] Jürg Dual,[2,*] and Collin Y. Ewald[1,4,*]

SUMMARY

Human centenarians and longevity mutants of model organisms show lower incidence rates of late-life morbidities than the average population. However, whether longevity is caused by a compression of the portion of life spent in a state of morbidity, *i.e.*, "sickspan," is highly debated even in isogenic *Caenorhabditis elegans*. Here, we developed a microfluidic device that employs acoustophoretic force fields to quantify the maximum muscle strength and dynamic power in aging *C. elegans*. Together with different biomarkers for healthspan, we found a stochastic onset of morbidity, starting with a decline in dynamic muscle power and structural integrity, culminating in frailty. Surprisingly, we did not observe a compression of sickspan in longevity mutants but instead observed a temporal scaling of healthspan. Given the conservation of these longevity interventions, this raises the question of whether the healthspan of mammalian longevity interventions is also temporally scaled.

INTRODUCTION

The continuously growing elderly population is projected to result in 1.5 billion people older than 65 years globally by 2050 (United Nations, Department of Economic and Social Affairs, Population Division, 2019). This poses a significant challenge, as old age is the major risk factor for developing cancer, dementia, cardiovascular, and metabolic diseases (Partridge et al., 2018), especially because people suffer for approximately 20% of their lifespan from one or multiple of these chronic illnesses, which are themselves accompanied by other late-life disabilities (Partridge et al., 2018). Current estimates indicate that delaying the onset of these chronic diseases by one year would save $38 trillion in the US alone (Scott et al., 2021). Therefore, major research efforts are dedicated to understanding how to increase the time spent in good health (*i.e.*, healthspan) and to postpone and compress the time spent suffering from age-related pathologies and chronic diseases (*i.e.*, sickspan) (Kaeberlein, 2017; Kennedy et al., 2014; Olshansky, 2018; Partridge et al., 2018).

People who are older than 100 years, so-called centenarians, display a delayed onset and a lower incidence rate of late-life morbidities compared with people in the age bracket of 80–89 years (Ailshire et al., 2015; Andersen et al., 2012; Evans et al., 2014; Evert et al., 2003; Ismail et al., 2016; Kheirbek et al., 2017). Genome-wide association studies have shown associations between the exceptional longevity of centenarians and aging-related genes identified in model organisms (Kenyon, 2010; López-Otín et al., 2013; Partridge et al., 2018). Mutations in genes that promote longevity in model organisms, such as *Caenorhabditis elegans,* have been instrumental in identifying mechanisms that promote healthy aging (Kenyon, 2010; López-Otín et al., 2013; Magalhães et al., 2017; Partridge et al., 2018).

A recent study has questioned this approach of using *C. elegans* longevity mutants to gain insights for promoting healthy aging or mechanisms that prolong healthspan (Bansal et al., 2015). Using four matrices (resilience to heat and oxidative stress, voluntary movement, and swimming performance) to assess the "health" status of aging *C. elegans*, they found that four commonly used longevity mutants outperformed wild type at any given time point at older ages, consistent with previous reports. However, compared with their maximum lifespan, longevity mutants displayed an increased sickspan-to-healthspan ratio compared with wild type (Bansal et al., 2015). Other studies have not observed an increase of sickspan in long-lived *C. elegans* mutants, except in the case of lower mobility or movement scores for the insulin/IGF-1 receptor longevity *daf-2(e1370)* mutants (Hahm et al., 2015; Huang et al., 2004; Podshivalova and Kerr, 2017; Stamper et al., 2018). Part of the "prolonged sickspan" based on the motility of these *daf-2(e1370)* mutants was attributed to lack of behavioral exploration linked to *odr-10* gene expression (Hahm et al., 2015) and

[1]Laboratory of Extracellular Matrix Regeneration, Institute of Translational Medicine, Department of Health Sciences and Technology, ETH Zürich, Schwerzenbach CH-8603, Switzerland

[2]Eidgenössische Technische Hochschule Zürich, Department of Mechanical and Process Engineering, Institute for Mechanical Systems, Zürich CH-8092, Switzerland

[3]These authors contributed equally

[4]Lead contact

*Correspondence:
collin-ewald@ethz.ch (C.Y.E.),
dual@imes.mavt.ethz.ch (J.D.)

https://doi.org/10.1016/j.isci.2022.103983

improper dauer-like quiescence behavior (Ewald et al., 2015, 2018; Gems et al., 1998; Hess et al., 2019; Podshivalova and Kerr, 2017). Although all these studies showed that sickspan is not increased in longevity mutants, the question remained about how healthspan changes when the lifespan is extended. We hypothesized that using other health matrices independent of voluntary or behavioral influences, such as physical properties of muscular strength, which is one of the best predictors for all-cause mortality in humans (Leong et al., 2015), we might be able to quantify the health trajectory of *C. elegans* longevity mutants.

Here we confirm that voluntary movement during aging declines, and this fragility is not extended in longevity mutants, except mildly in *daf-2* mutants, using high-resolution lifespan and movement measurements on plates. We developed a novel microfluidic device and applied acoustophoretic force fields to quantify the maximum force and power of *C. elegans*. Using a high-frequency and high-power acoustic force field, it becomes possible to set up a contactless, constant in time, and uniform force field acting along the whole *C. elegans* body. Therefore, this force field challenges swimming *C. elegans* in a similar way body-weight exercises do for humans in a gravity field. Furthermore, applying the acoustic field stimulated a swimming response of resting *C. elegans*. All longevity mutants showed delayed onset of the decline in maximum force and dynamic power during aging. We observed heterogeneity between individuals across all genotypes in the onset of age-related phenotypes, several correlated phenotypes, and a time-dependent occurrence of multiple disabilities. However, we did not find a compression of sickspan but rather a temporal scaling of healthspan relative to their maximal lifespan across genotypes.

RESULTS

Voluntary movement healthspan is proportionally increased by longevity interventions

To obtain highly quantitative data on lifespan and healthspan, we used a lifespan machine (Stroustrup et al., 2013). Here, we defined the "voluntary movement healthspan" as the time spent fast crawling and the "voluntary movement sickspan" as the time spent slow crawling or displaying minimal posture changes (see Voluntary movement healthspan measured by lifespan machine for detailed definition). We chose *eat-2(ad1116)* as a genetic model for dietary restriction-like longevity, *glp-1(e2141)* as a genetic model for germ-stem-cell-less-mediated longevity, and *daf-2(e1368)* and *daf-2(e1370)* as genetic models for reduced insulin/IGF-1-signaling-mediated longevity. We cultured all animals at the same temperature (15°C) and in the same environment with the same food source, except *glp-1* that underwent a brief temperature upshift during development as in preparation for the lifespan assay. To avoid dauer-specific traits that occur in reduced insulin/IGF-1 signaling mutants (Ewald et al., 2018) and to avoid pathogenicity from a bacterial food source (Podshivalova and Kerr, 2017), lifespans were run at 15°C on heat-killed bacteria. Thus, the experimental setup was designed to offer optimal conditions and was kept identical while *C. elegans* genotypes were varied.

As expected, we measured a significant increase in lifespan for these long-lived mutants compared with wild type (Figure 1A; Table S1 and Video S1). Under our experimental settings (heat-killed bacteria), the *eat-2* longevity was shorter as previously reported on live bacteria but in line with previous findings that had demonstrated that *eat-2* predominantly extends lifespan by lowering the proportion of deaths caused by invasion of the pharynx from live bacteria (Zhao et al., 2019). Interestingly, our data showed that the longer-lived the mutant was, the more prolonged was the voluntary movement healthspan (Figure 1B). Therefore, interventions that increase lifespan also increase the time spent moving fast and actively.

Relative increase for both healthspan and sickspan in long-lived mutants

To better understand the rescaling of the time spent in frailty in these long-lived mutants, we analyzed the fraction of slow-moving animals per day. We observed Gaussian activity distributions, which were shifted along the time axis for these longevity mutants (Figure 1C). This delayed onset of the sickspan (Figure 1C) is consistent with the prolonged healthspan of these long-lived mutants (Figure 1B). However, except for *eat-2* and *glp-1* mutants, the width and the area of the Gaussian distributions were bigger for long-lived mutants than wild type (Figure 1C), suggesting an overall increase of sickspan. Thus, based on voluntary movement tracking, long-lived mutants display increased absolute healthspan and absolute sickspan compared with wild type. Next, we asked whether the fraction spent in healthspan and sickspan during the lifespan is altered. Wild-type animals spent 78% of their lifespan fast-moving and 22% slow-moving (Figure 1D). For long-lived mutants, we recorded about 70%–79% of their lifespan are spent fast-moving (Figures 1D and S1), suggesting no compression of sickspan but rather a proportional scaling of both healthspan and sickspan relative to their lifespan.
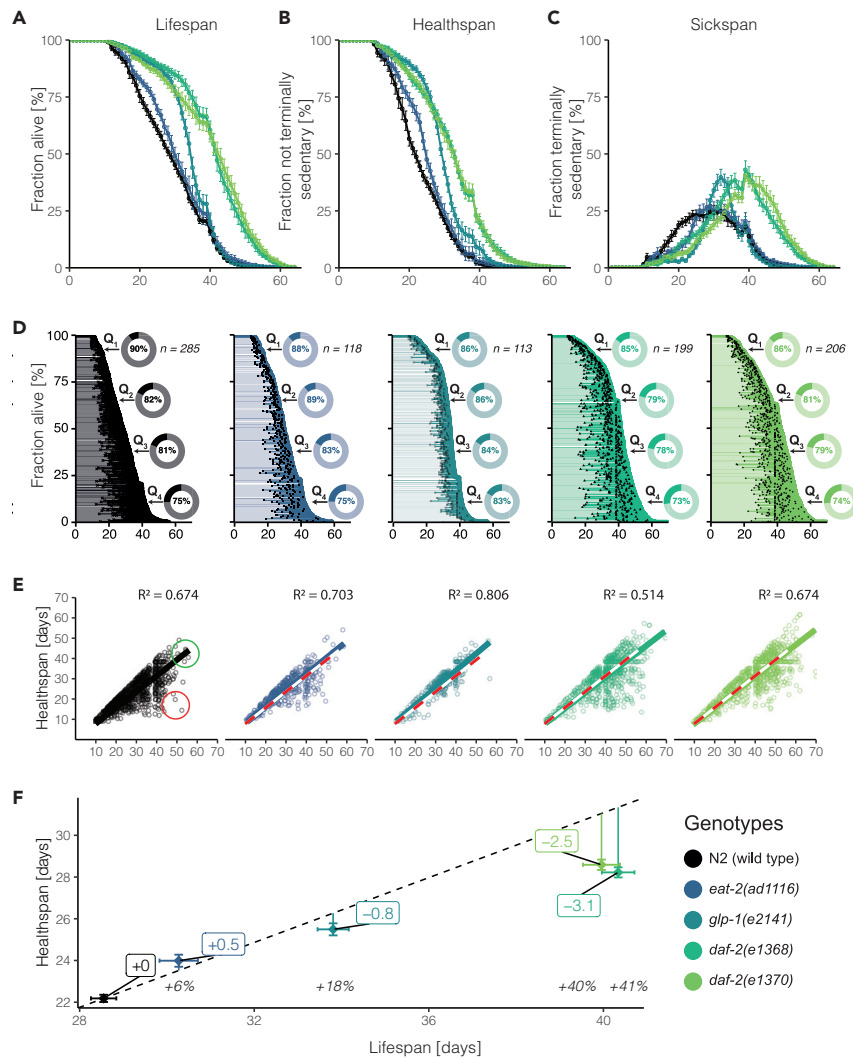
Figure 1. Voluntary movement quantification in aging *C. elegans* populations

C. elegans lifespan analysis displaying survival (A), healthspan (B), and sickspan (C) for each genotype. Error bars, SEM between plates at 24-h intervals. Healthspan refers to the time span of fast movement, sickspan to the time spent in sedentary movement, and lifespan to the time until the animal fails to move irretrievably. The area under the curve (AUC) relative to N2 was 0.9 for *eat-2*, 0.8 for *glp-1*, 1.54 for *daf-2(e1368)*, and 1.46 for *daf-2(e1370)*. The fate of each individual is displayed separately for each genotype overlayed with the population's survival (D). Here, each individual's healthspan is marked as a transparent line spanning from young adulthood to the onset of sickspan marked by a black dot and then extends further as sickspan until the individual's point of death on the population survival curve. The inset displays the overall proportion each genotype spends in their healthspan for each lifespan quantile (Q_1–Q_4). The correlation between health and lifespan is shown in figure (E). Each individual is represented as a point with its lifespan on the x axis and its corresponding healthspan on the y axis. A linear model passing through the origin is shown as a solid line. The wild-type (N2) model is superimposed on the longevity mutants as a red and white dashed line. All genotypes are compared with temporarily scaled wild-type N2 with the mean population lifespan and healthspan and error bars indicating the standard errors (F). The extrapolated ratio of healthspan to the lifespan of wild type (0.78) is displayed as a dashed black line. The distance of each population average is marked by a vertical line, and the difference in expected healthspan is indicated.

Heterogeneity in the length of sickspan but a fixed onset of sickspan

Because we did not observe a compression of voluntary movement sickspan of the entire population, we wondered whether individual animals that outlived their siblings would display a compressed sickspan. When we compared the sickspan traces of individual *C. elegans* for each genotype, we were surprised to measure such a vast heterogeneity (Figure 1D), given that all these individual animals of a population are genetically identical, consume the same food, and are housed in the same environment. Only the

glp-1-mediated longevity showed an overall compression of individual sickspan traces (Figure 1D). For comparison among these different genotypes, we decided to use "relative age" by dividing lifespan curves into quartiles and computing the healthspan to sickspan ratio for each quartile (Figures 1D insets and S2). Consistent with previous reports on wild type (Zhang et al., 2016), we found that in the first quantile of the lifespan curve, individual animals spent about 90% of their lifetime fast-moving and 10% slow-moving, indicating that these animals die young with a compressed sickspan compared with the last quartile wherein animals spent about 75% of their lifetime fast-moving and 25% slow-moving (Figure 1D insets and S1). Remarkably, it looks like the onset of an individual's sickspan is a fixed event starting approximately when the first 10% of the isogenic population starts to die (Figure 1D). This observation suggests that up to a certain time point, the animal's physiological integrity is maintained. After this time point, there appears to be a stochastic decay, resulting in a heterogeneous sickspan distribution. Viewing the data using this alternative interpretation of a fixed onset of sickspan would explain why animals in the first quartile of the lifespan curve die young and spend less time in poor health, whereas animals in the last quartile of the lifespan curve die old and spend more time in poor health. Thus, the time spent fast-moving versus slow-moving seems to have a fixed onset in time.

Voluntary movement healthspan temporally scales with lifespan except in *daf-2* mutants

The model of a fixed onset-time point for frailty would suggest that longevity interventions would simply delay the onset. To address this, we contrasted the number of days spent fast-moving (healthspan) for each individual as a function of their time lived (lifespan in days; Figure 1E). We found that the time lived correlated and predicted the time spent fast-moving with an R squared of 0.7 for wild type and R squared ranging from 0.5 to 0.8 for the longevity mutants (Figure 1E). Furthermore, the *glp-1* with an R squared of 0.8 and *daf-2(e1368)* with an R squared of 0.5 indicate lower or higher heterogeneity, respectively, compared with wild type (Figure 1E). This is also apparent in the increased or decreased spread of data points below the regression line in Figure 1E and by increased or decreased lengths of the individual sickspan traces in Figure 1D, respectively. One interesting aspect to note is that individuals in quartiles 2 and 3, which expire in the middle of the lifespan curves, displayed shortened healthspan relative to their lifespan, whereas individuals in the last quartile showed an extended healthspan relative to their lifespan (Figure 1E). This might be because sicker individuals simply died earlier, leading to an enrichment of healthier-aging individuals in the last quartile (Figures S1 and S2). Based on the high R squared values for all genotypes, we applied a linear model to investigate the relationship between healthspan and lifespan (Figure 1E). Steeper linear regression lines compared with wild type would indicate an increase in healthspan to lifespan ratio. The slopes of the linear model were steeper for *eat-2* and *glp-1* but less steep for the two *daf-2* mutants compared with wild type (Figure 1E), suggesting that *glp-1* and *eat-2* spent a larger fraction and *daf-2* mutants spent a smaller fraction of their lifespan actively moving. Because slopes of linear models can be sensitive to extreme values, we compared the population means of healthspan and lifespan across all genotypes (Figure 1F). When we extrapolated the mean healthspan to mean lifespan ratio of wild type, we found that *eat-2* and *glp-1* were close to this extrapolated line, whereas the *daf-2* mutants lacked approximately three days (*i.e.*, 7%) of mean healthspan with respect to their mean relative lifespan (Figure 1F). To demonstrate that all these measurements are true under other experimental settings, we chose temperature-sensitive sterile mutant *spe-9(hc88)* to compare with *glp-1(e2141)* that were raised at 25°C until day two of adulthood to avoid progeny and then kept for the remainder of their lifespan at 20°C and quantified comparable results (Figure S3). Thus, we uncovered that the prolonged voluntary movement healthspan temporally scales with the prolonged lifespan for each of these longevity mutants except less stringently for *daf-2* mutants.

Acoustophoretic characterization of *C. elegans* force and muscle power

Thus far, our observations and interpretations on healthspan are based on the decline of voluntary movement on culturing plates in the abundance of food. Certain genotypes like *daf-2(e1370)* are less motivated to forage and display a more rapid decline in voluntary foraging behavior compared with wild type, leading to the interpretation of being less healthy (Hahm et al., 2015). In our setting, this lower foraging behavior is less pronounced in *daf-2(e1370)*, as they were cultured at 15°C, an environment that avoids improper dauer program activation (Ewald et al., 2018). To overcome this, we developed an inducible and motivation-independent exercise platform for *C. elegans*. Our goal is to address the following shortcomings of current methods: the movement should be inducible with a strong stimulus and not dependent on secondary cues such as food or intrinsic motivation; it should be measurable in a short time window to assess health in this instant, and it should directly measure a physiologically relevant

parameter such as maximum muscle force or functional tissue integrity. This is especially important when comparing different genotypes, which often respond differently to their environment.

In humans, one of the best predictors for all-cause mortality is the decline in muscle maximum force and power (Kostka, 2005; Leong et al., 2015; Petrella et al., 2005). However, a tool or device to quantify the maximum force and power of *C. elegans* muscles did not exist. The application potential would be immense, as *C. elegans* muscle structures are strongly conserved, as in mammals, and forced maximum strength measurements to the point of collapse would be unethical in mammalian models. We developed a microfluidic device harnessing the power of acoustic standing waves (Figures 2A and 2B and Video S2). We have recently applied ultrasonic waves to compress, move, and quantitatively characterize larval *C. elegans* (Baasch et al., 2018). We reasoned that we could employ ultrasonic standing waves to trap and stretch out *C. elegans* in the minima of the acoustic force fields (Figures 2C and 2D). *C. elegans* dislike being trapped and try to escape by applying mechanical forces (body bending) against the acoustic force field (Figures 2C and 2D). The further away from the acoustic force field minimum, the harder it gets to move against the force field (Figure 2D). Suppose the animal is stronger than the applied acoustic force field. In that case, it can turn around in the microfluidic chamber (Figure 2C), typical escaping behavior of *C. elegans* known as omega reversals (Donnelly et al., 2013). Thus, the degree of deflection of the *C. elegans* body away from the acoustic force field minimum provides an estimate of the maximal muscle strength the animal can master to try to escape the acoustic trap.

Muscular strength declines in aging *C. elegans*

To quantify muscular forces, we developed a model by dividing the *C. elegans* body plan into 13 rigid links connected by joints along the animal's midline (Figure 2E). Upon applying acoustic force fields, we measured the deflection of these 13 nodes for 30 s and the number of times the animal escaped the force fields (Figure 2F). A typical exercise round is structured in up to ten cycles consisting of 30 s of ultrasonic force and a 5-s break (Figure 2G). We measured the muscular forces of aging wild-type *C. elegans* (Figure 2G). After three to five cycles, we observed muscle fatigue, which set in earlier the older the animals were (Figure 2G). We observed first an increase and then a decrease in the heterogeneity of individual *C. elegans* muscular strengths (Figure 2G). Similarly, we first saw an increase and then a progressive decline in muscle power during aging (Figure 2G). By contrast, we found that longevity mutants performed better in terms of muscle strength and function at day 20 of adulthood (Figure 2H); this indicates the preservation of muscle power in aging longevity mutants.

Longevity mutants showed prolonged healthspan assessed by the strength performance in longitudinal comparison to wild type

The overall force and power of a *C. elegans* depend on its muscle strength as well as its total body size. In agreement with previous reports (Hulme et al., 2010; Shi and Murphy, 2014), we observed adult *C. elegans* kept growing in body size beyond the reproductive period and then shrunk during aging (Figures 3A and 3B). A prolonged growing phase correlates with longevity (Hulme et al., 2010). We found that longevity mutants prolonged their growing phase and shrunk less than wild-type animals during aging (Figures 3A and 3B). Structural integrity declines during *C. elegans* aging, such as internal organ atrophy (Ezcurra et al., 2018), loss of internal pressure (Gilpin et al., 2015), and disorganization of the exoskeleton cuticle (Essmann et al., 2020). We noticed that in the acoustic force field, *C. elegans* undergoes compression, and this compressibility stays fairly constant during aging (Figures 3C and 3D). We conclude that although morphological changes occur during aging, the mechanical properties regarding compression are less affected by age, and this points toward muscular strength playing a pivotal role. On average, young *C. elegans* can overcome the acoustic force field leading to an omega turn eight times each cycle (Figure 3E and Video S3). The ability to overcome the force field and turn in the microfluidic chip progressively declines during aging but is preserved in longevity mutants (Figures 3E and S4). Turning in the chip can be viewed as a measure of high-intensity muscular capacity, as the animal can completely overcome the force field. It also showcases that the animal is not placid but trying to escape. Next, we assessed the overall energy per individual *C. elegans* as an assessment of overall body volume deflected against the force field. We found an increase of energy per individual until mid-age and then a decline (Figure 3F) reminiscent of the longitudinal body size curve (Figure 3G). In our measurements to determine the overall force and power of *C. elegans*, the body size is a confounding factor. In all our longitudinal measurements, we had included a positive control in the form of a muscle-defective mutant (CB190) that carries a mutation in the muscle myosin class II heavy chain (*unc-54*). These muscle-constriction-defective mutants were unable to perform
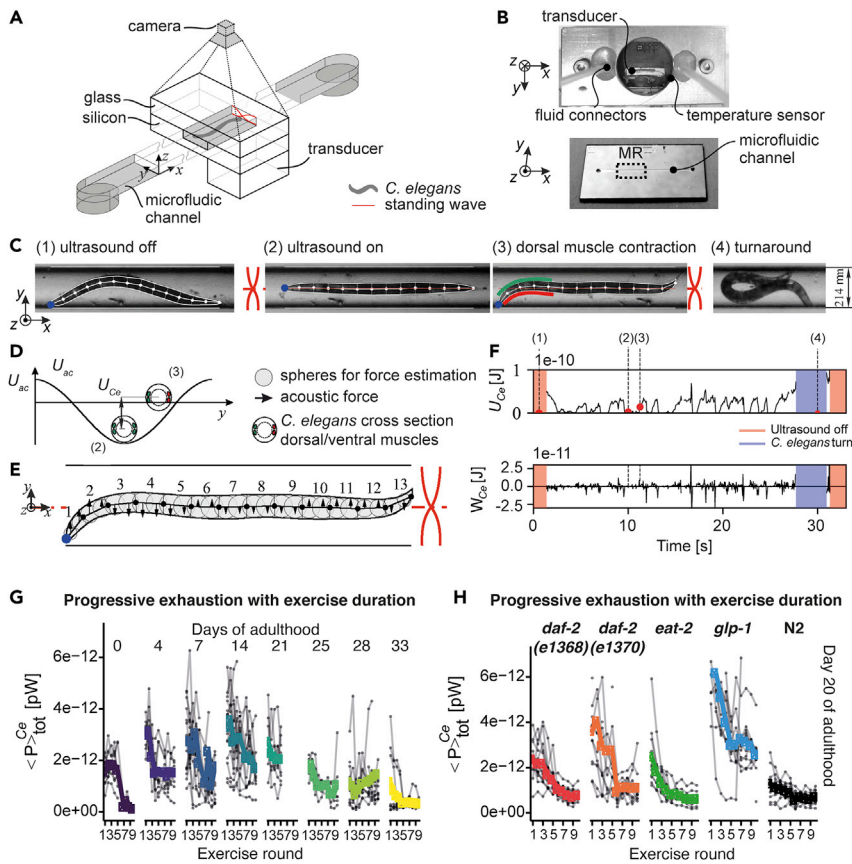
Figure 2. Experimental setup to measure maximum *C. elegans* muscle strength

Top view of the schematic representation of the silicon/glass acoustofluidic chip, fluid inlets and outlets, and the piezoelectric transducer positioned at the bottom and *C. elegans* trapped in the standing wave (A). A photograph of the back of the chip together with the metal clamps, the attached fluid connectors, temperature probe, and a piezoelectric transducer is shown (B, top). The front view of the chip provides an overview of the device shape, the microfluidic channel, and the measurement region (MR) (B, bottom). A day 4 wild-type *C. elegans*, as seen by the camera in the measurement region, is displayed together, with the image processing output highlighting the outline and the segmented midline of the animal as well as the channel borders and centerline (C). The effect of the acoustic field (frequency: 3.543 MHz, voltage amplitude: 76 Vpp, $\lambda/2$ mode) is shown in (C, 2), aligning the animal at the midline. The animal exercises maximum muscle power attempting to bend its head away from the midline (C, 3) to achieve a turn (C, 4), likely as an attempted escape response. The working model to quantify the *C. elegans* muscular force consists of 13 rigid links along the animal's midline, which are connected by joints. Blue arrows reflect the muscle activity acting on each joint to generate a force against the acoustic field (E). The acoustic force acting along the animal's body is modeled as the individual acoustic forces acting on the gray spheres aligned along the body and represented by black arrows, with the length of each arrow being proportional to its force or moment magnitude. The acoustic radiation potential is illustrated using a *C. elegans* cross-section highlighting the animal's four body wall muscles (D). If stretched, the animal rests at the minimum (see C 2) and, upon muscle contraction, moves upward in its potential energy well (see C3). The four *C. elegans* frames (C 1–4) are put in the context of one 30-s actuation cycle showing the time-resolved total energy and mechanical work quantification for this animal (F). Red areas reflect regions of zero energy due to the acoustic field being turned off, and the blue areas indicate *C. elegans* turn movements during which muscle force estimation is paused. A *C. elegans* maximum force assessment routine consists of multiple 30 s exercise rounds intermitted by 5-s breaks for a total of up to ten actuation cycles. For wild type, this exercise regimen is displayed with the exercise rounds on the x axis and the total power (time-averaged) on the y axis, as derived from the respective total energy curve in (F) and the age of the population given at the top of each facet (G). Wild-type *C. elegans* is contrasted to long-lived *C. elegans* genotypes across up to ten exercise rounds focusing on the aged cohort above day 20 of adulthood (H).

omega turns in the chip but showed similar compressibility and longitudinal growth curves, illustrating that the rise and fall of the overall energy are confounded by the organismal growth curve. Therefore, we decided to use the dynamic power as defined as energy expenditure relative to the previous time point and normalized it by the volume of each animal (*i.e.*, volume; Figure 3H). Using a human analogy, total

A wild type (N2)

0
8
14
18
28
33

Age [Days of adulthood]

B *daf-2(e1368)*

0
8
14
18
28
33

Age [Days of adulthood]

C Median length of each individual animal

N2 *daf-2(e1368)* *daf-2(e1370)* *eat-2* *glp-1* CB190

Animal's length [μm]

D Volume for each individual

N2 *daf-2(e1368)* *daf-2(e1370)* *eat-2* *glp-1* CB190

Volume [m³]

E Number of turns per individual

N2 *daf-2(e1368)* *daf-2(e1370)* *eat-2* *glp-1* CB190

turns

F Median energy per individual

N2 *daf-2(e1368)* *daf-2(e1370)* *eat-2* *glp-1* CB190

Overall energy [pJ]

G Effect of the acoustic field on animal's diameter

N2 *daf-2(e1368)* *daf-2(e1370)* *eat-2* *glp-1* CB190

Individual phenotypes

H Effect of the acoustic field on animal's volume

N2 *daf-2(e1368)* *daf-2(e1370)* *eat-2* *glp-1* CB190

Individual phenotypes

I Dynamic power / volume

N2 *daf-2(e1368)* *daf-2(e1370)* *eat-2* *glp-1* CB190

$\langle P \rangle^{Ce}_{dyn} / V$ [W / m³]

30% 83% 61% 55% 82% 0%

Age [Days of adulthood]

Strain
N2
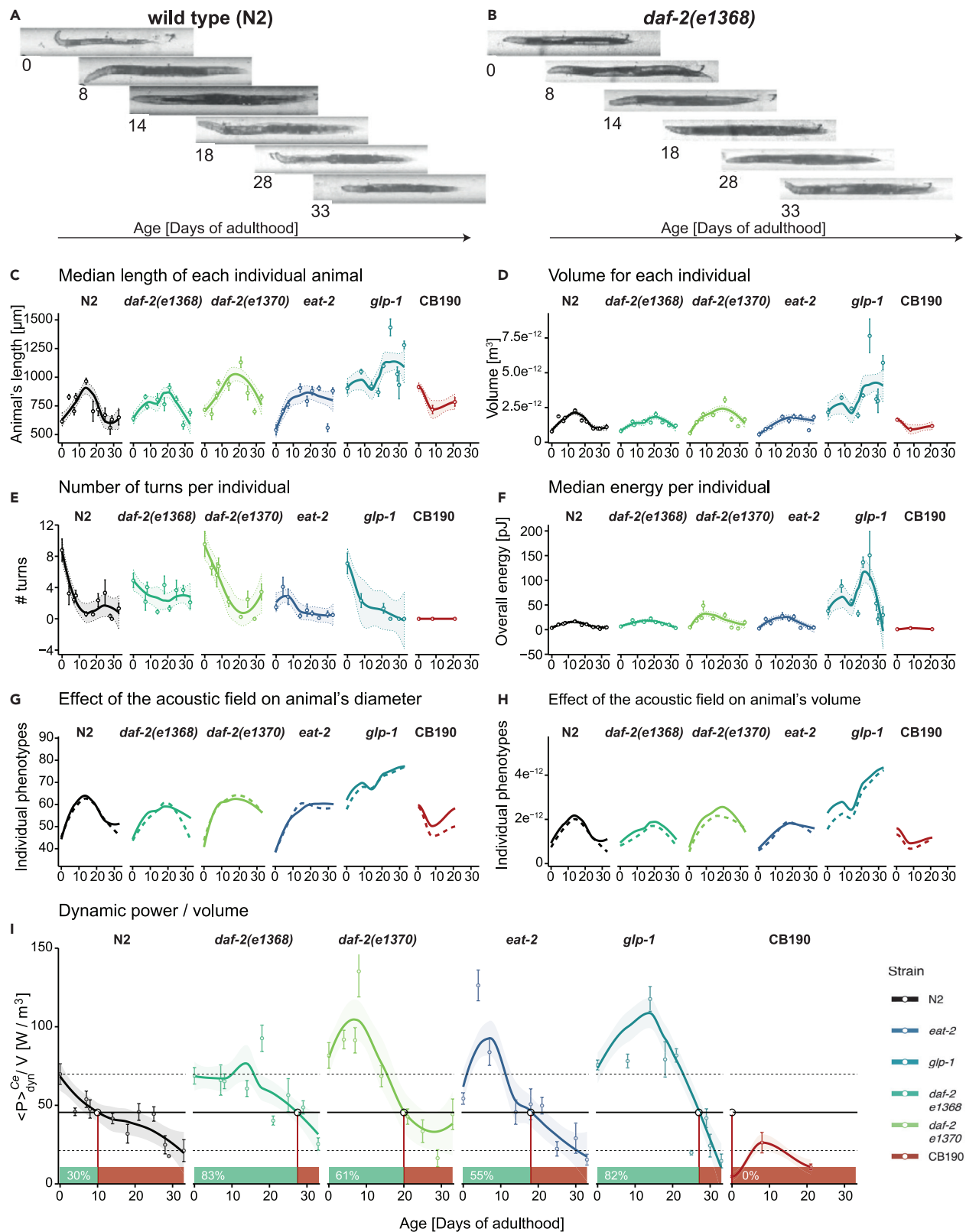*eat-2*
glp-1
daf-2 e1368
daf-2 e1370
CB190

Figure 3. Time course of fitness- and structural-related phenotypes for wild-type and long-lived *C. elegans* under acoustic stimulation

Acoustic compression was used to quantify phenotypes directly (# turns, energy, diameter and volume compression, and dynamic power by volume) as well as indirectly by exploiting the nondestructive linear alignment of the animals (length, volume). Randomly selected images for N2 (A) and *daf-2(e1368)* (B) at different ages are displayed to illustrate the positioning of the *C. elegans* in the microfluidic measurement channel and how all matrices are shown below were obtained. Measurements are displayed as mean ± SE for each assessed age point and subjected to local polynomial regression fitting displayed as a full line with the CI set to 95% and bounded by dashed lines. For the acoustic compression only, the fitted line is shown. The length (C) and volume (D) of the animal was quantified automatically using the entire length and area of the animal in the channel, respectively. The number of turns was quantified manually and corresponded to the number of times an animal successfully changed its orientation in the channel by 180°. The total energy of the individual was calculated using the magnitude of the lateral deflection of the animal from the channel middle (F). The compression experienced by the animal diameter (G) and volume (H) when the field is activated was computed automatically and displayed as a full line when the field is on and a dashed line when the field is off. The dynamic power/volume (I) reflects the work the animal performs against the field to change its lateral position in the channel and is normalized by the overall volume of the animal to enable comparisons across genotypes making this the most informative health parameter. The mean value for day 0 and day 33 N2 animals are indicated in black dashed lines, and the half-activity value between these two extremes is shown as a full line, which is also used to deduce the healthspan to sickspan transition for each genotype. Using this N2 half-activity value, the individual strains reach their sickspan at approximately 10 days for N2, 28 days for *daf-2(e1368)*, 20 days for *daf-2(e1370)*, 18 days for *eat-2(ad1116)*, and 27 days for *glp-1(e2141)*, whereas CB190 *unc-54(e190)* spends its entire lifespan in its sickspan fraction. Long-lived genotypes, in general, do not experience the same linear energy density decline as wild type, as their total energy decrease is slowed down, as is their growth leading to a nonlinear energy density trajectory.

refers to how long a weight can be lifted, dynamic power only considers the process of lifting the weight without holding the weight, and dynamic power takes the weight of the person lifting the weight into account. In this way, we found that the overall force and power of longevity mutants were preserved for almost three-quarters (55%–83%) compared with about one-third (30%) of their lifespan in wild type (Figure 3I). Thus, muscular strength is maintained longer in longevity mutants.

Temporal scaling of age-related pathologies in longevity mutants

Next, we asked whether other age-related pathologies or morphological changes show any delayed onset in longevity mutants compared with wild type. We quantified 592 animals, investigated time points between day 0 and day 33 (12 animals on average per strain and time point) at the first two cycles of actuation (1183-time sequences), which comprised over 800'000 frames in total. We then manually quantified additional morphological changes such as intestine length and diameter, pixel intensity, wrinkles in the cuticle, and pharynx diameter in a subsampled representative subset (approx. 50'000 frames; Figure S5). Although not all, many age-related phenotypes were delayed in their onset and displayed a slowed decline in longevity mutants compared with wild type (Figures 4A, 4B, and S6). Rescaling phenotypic trajectories of wild type by the lifespan extension observed in the long-lived strains revealed that many closely match the trajectories observed in long-lived strains for both *daf-2* mutants (Figure 4C). Notably, for animals' length, diameter, volume, and intestine length, phenotypic scaling was observed when comparing wild type with *daf-2(e1368)* and *daf-2(e1370)*. In the case of *eat-2*, the observed lifespan extension was too limited to draw conclusions, and *glp-1* never ceased growing. The severely paralyzed myosin mutant *unc-54(e190)* displayed the opposite phenotypic trajectories than all other genotypes (Figure 4C). When approximating the phenotypic trajectories as segmented linear fit reflecting the separated phases of growth and decline, we observed that the starting values as young adults are often similar (Figure 4C). However, the slopes and point of decline are shifted compared with wild type.

Investigating each phenotype in isolation is hindered by the inherent noise in the measurement as well as by the incomplete picture each phenotype provides. Furthermore, many phenotypes such as length, diameter, and volume were strongly correlated. For this reason, we subjected all phenotypes to principal component analysis (PCA) to study the overall age trajectory (Figure S7A). We traced these phenotypes of all genotypes across the PCA plot as they age (Figure S7B). All physiological parameters increased from young to middle-aged and then reverted again as the animal reached old age. However, muscle strength density decreased steadily. Using the paralyzed mutant, we were able to establish the bottom left quadrant as a reduced health area; this was only possible when using both physiological and performance measurements and was entered only by the paralyzed strain as well as old wild-type animals. The multi-phenotype traces are also shown for each genotype individually (Figures S7C and S7D). Taken together, this suggested that many of these phenotypes change similarly during aging, that many are temporally scaled in longevity interventions, and that maximum muscle strength offers an orthogonal perspective on studying aging compared with physiological features; this highlights the importance of performing high-intensity muscle strength measurements when studying physiological aging and quantifying healthspan.
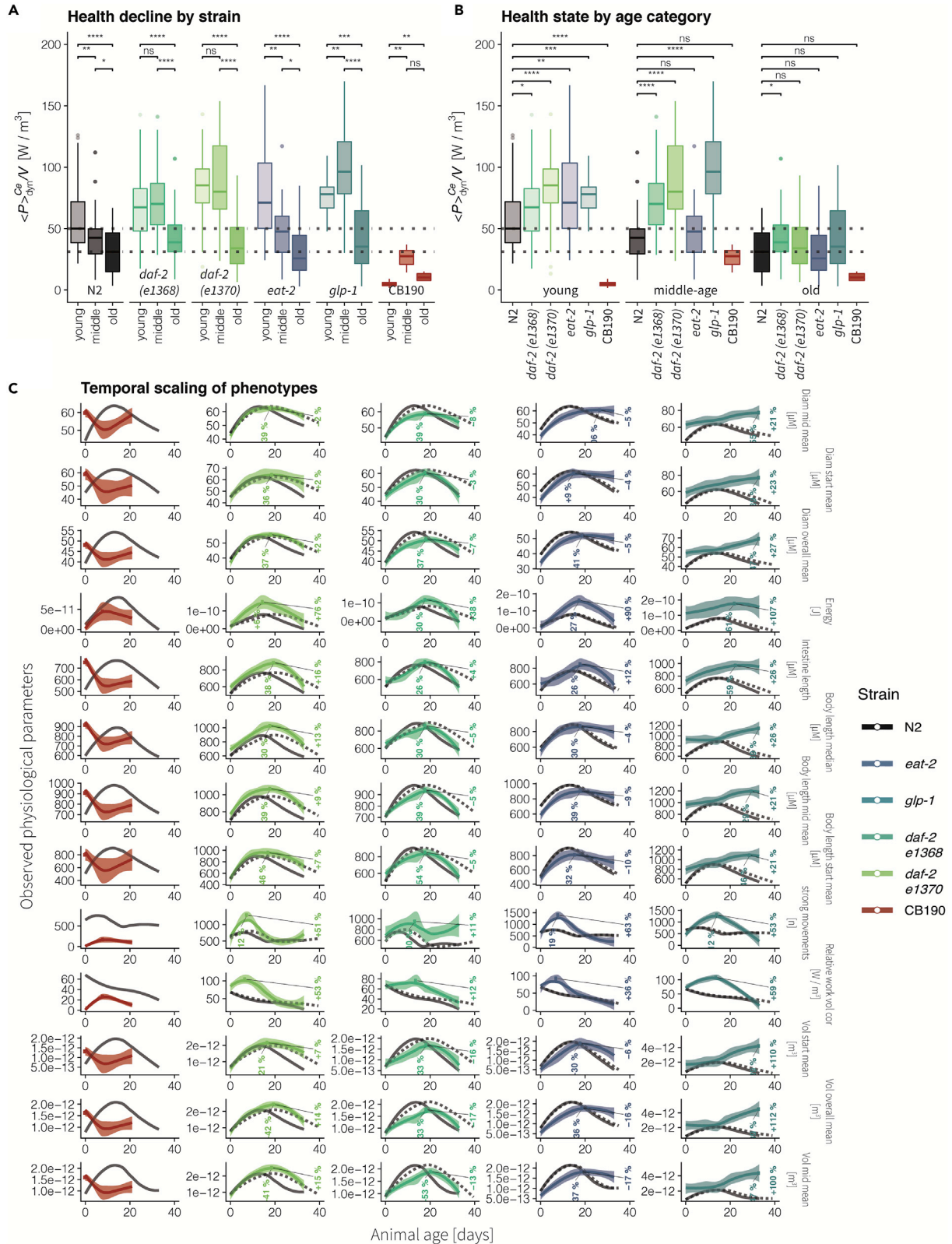
A Health decline by strain

B Health state by age category

C Temporal scaling of phenotypes

Figure 4. Temporal scaling of *C. elegans* aging phenotypes

The measured values of selected phenotypes are shown using different scales on the y axis, animal age on the x-axis, and facetted by strain (A). To address the temporal scaling of phenotypes hypothesis, the loess fit of the measured values for wild type is shown as a solid gray line, and its temporally scaled values using the respective mean lifespan increase experienced by the respective strain are shown as a dashed line also in gray. The measured phenotype trajectory for each strain is shown in color, each in a separate panel. The maximum fitted value is marked using white point, and its increase relative to the maximum fitted values measured for wild type is shown for both the age and phenotype variables. The same phenotypes as in inset (C) are modeled using a piecewise linear relationship in (B). The breakpoint of the segmented fit is estimated by the model at the age value, where the linear relationship between the measured phenotype and population age changes. The individual animals measured at each time point are displayed as mean +/− SE.

Longevity mutants show prolonged absolute but not relative healthspan

Our data revealed that longevity mutants stay healthier compared with wild type and experience a slower decline in physiological integrity. Indeed, dividing the lifespan of each genotype into three chronological fixed age categories—young (younger than 7 days), middle (older than eight but younger than 19 days), and old age (>20 days of adulthood)—showed a progressive decline of volume-corrected work performed (Figures 5A and 5B). Longevity mutants performed better in the middle age group than wild type, but only *daf-2(e1368)* outperformed wild type in the old age group (Figures 5A and 5B). Using hierarchical clustering of temporally scaled phenotypes as a complementary analysis, we found that longevity mutants often cluster with chronologically younger wild-type samples (Figure S8).

Integration of voluntary movement and forced maximum muscle strength quantification to yield a comprehensive understanding of *C. elegans* healthspan

Having two independent assessments of healthspan that act on very different stringency levels, we can further divide *C. elegans* healthspan into three divisions: prime health (passes both matrices), fragile health (passes one metric), and sickspan (failing both matrices) (Figure 5C). Consistent with previous observations in other species, the maximum power drops prior to the cessation of general mobility (Kostka, 2005; Leong et al., 2015; Petrella et al., 2005). Muscle performance is much more improved in longevity mutants in relation to wild type compared with the voluntary movement (Figure 5C). Integrating both matrices revealed that wild type spent around 16% of their lifespan in prime health, whereas longevity mutants spent double the time in prime health (28%–42%; Figure 5C). From all four longevity genotypes, *daf-2(e1368)* appears to be the healthiest strain (Figure 5C). Thus, combining multiple matrices of physiological and behavioral integrity is a powerful assessment of healthspan.

DISCUSSION

Temporal scaling of healthspan

Understanding the relationship between healthspan and lifespan is an important question in aging research, as geroscience aims to increase the time spent in good health and to postpone and compress the time suffering from age-related pathologies and chronic diseases (Kaeberlein, 2017; Kennedy et al., 2014; Olshansky and Carnes, 2019; Partridge et al., 2018). Model organisms such as *C. elegans* are used to identify longevity-promoting interventions that can then be of translational value for humans (Kenyon, 2010; Magalhães et al., 2017). There is a fierce debate whether *C. elegans* longevity interventions show compression of sickspan and are of translational value for improving healthspan or healthy aging in humans (Bansal et al., 2015; Hahm et al., 2015; Huang et al., 2004; Podshivalova and Kerr, 2017; Stamper et al., 2018). In this study, we set out to develop a robust method to quantify maximum muscle strength as a highly interpretable healthspan metric with translational value. Lifespan measurements are well established and allowed the study of hundreds of lifespan-extending compounds and genetic alterations, leading to ground-breaking discoveries. However, this development is not reflected in the area of healthspan extension. Numerous methods exist that often measure proxy phenotypes for healthspan that are also motivation dependent such as pharyngeal pumping, thrashing, and others. With our approach, we were able to directly quantify muscle health in *C. elegans*; this is especially relevant, as *C. elegans* is an ideal model system for large-scale genetic screening, and both the microfluidic device as well as the image detection can be multiplexed. This approach could translate to the much-needed identification of (muscle) health-promoting interventions.

Combining acoustophoresis and microfluidics to quantify healthspan

The microfluidic device operates using acoustophoresis to generate an acoustic force field to quantify the physical fitness and muscle strength of aging *C. elegans*. Using different ways to assess healthspan in forms of voluntary movements, muscular force, muscular fatigue, structural integrity/compressibility, and
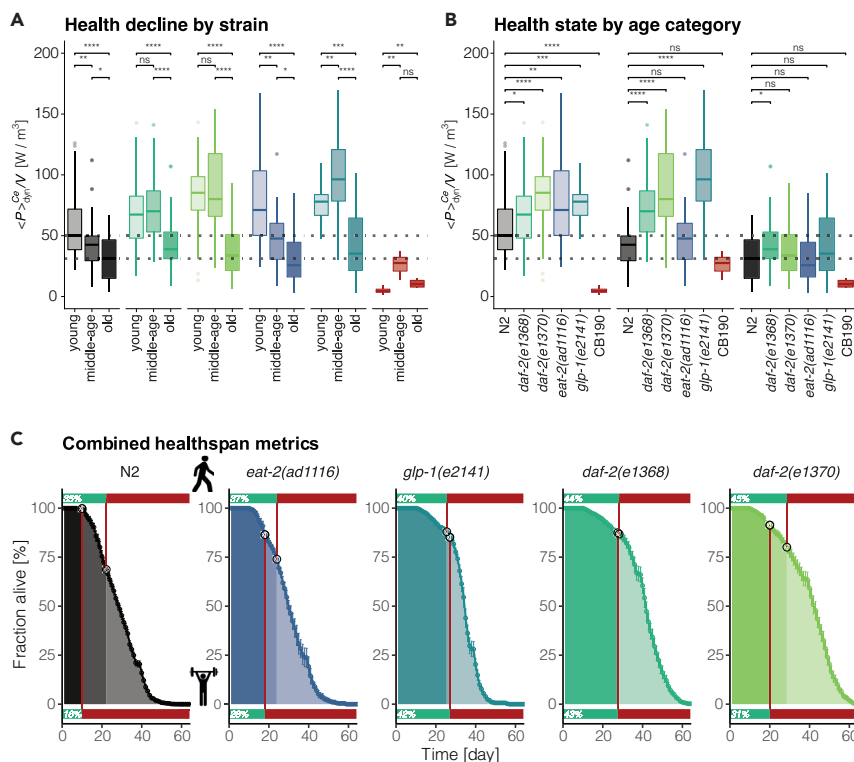
Figure 5. Integration of voluntary movement and forced maximum muscle strength quantification to yield a comprehensive understanding of *C. elegans* healthspan

The volume-corrected relative work performed by each genotype and grouped by age category (young ≤ 7 days, 8 < middle <20 days, old ≥ 20 days) is shown as boxplots facetted by genotype (A) and by age category (B). *P*-values of selected comparisons (Mann-Whitney test) are displayed as symbols (ns > 0.05, * <0.05, ** <0.01, *** <0.001, **** <0.0001). The Population medians for young and old N2 are displayed as horizontal dashed lines across all panels. (C) The measured lifespan of each *C. elegans* genotype is displayed with animal age on the x axis, the fraction of the population that is alive on the y-axis, and the mean +/- SE between plates shown as point and line range. The voluntary movement was quantified using the active versus sedentary behavior of the unstimulated animals on plates and is shown for each population as a bar at the top of each panel. Muscle health and the corresponding onset of sickspan due to reduced muscle function is depicted as a bar at the bottom of each facet. The position on the lifespan curve corresponding to the health-to-sickspan transition of either the unstimulated or stimulated healthspan quantification is marked by a white circle. The two health assessments divide the lifespan curve into three segments, with decreasing health status reflected by increasing transparency.

quantifying several age-related morphological changes, including cuticle/skin wrinkles, body, and internal organ sizes, we find that most of these phenotypic changes are postponed in longevity mutants. We observed a hierarchical and time-dependent succession in the occurrence of these phenotypes, starting with a decline in maximal force as indicated by overcoming acoustic field (omega turns), a decline in dynamic power, seizing of body and organ growth (intestine), and then decline in voluntary movement and becoming inactive and lethargic. Using PCA, we show that many of these phenotypes are strongly cross-correlated. The delay of all these age-related phenotypic changes is evident when using chronological age as a reference point for comparison of longevity mutants with wild type but disappears when using relative age as a reference; this points to the idea of temporal scaling of the healthspan. Consistent with this idea, we find that sickspan is neither compressed nor prolonged in longevity mutants compared with wild type. Thus, our quantifications suggest that *C. elegans* healthspan undergoes temporal scaling in longevity.

Limitations of the study

Aging is defined as a set of phenotypes or senescent pathologies occurring with a higher proportion in older individuals (Freund, 2019). Which senescent pathologies limit the lifespan depends on the context

and are different for different species, genotypes, and environments (Freund, 2019; Gems, 2015). Whether our chosen set of phenotypes assessed are directly limiting or affecting lifespan is unclear. However, it is evident that not one single mechanism underlies all our measured age-related phenotypes. On the other extreme, we do not observe a "one mechanism causing one age-related pathology" mechanism. Our data show that some phenotypes correlate and also follow a hierarchal time-dependent order of occurrence, indicating that these senescent pathologies are interconnected; this favors a mixed model of several causal mechanisms affecting multiply connected and independent senescent pathologies/phenotypes, including lifespan limiting phenotypes (Freund, 2019; Gems, 2015). Even if we might not measure lifespan limiting phenotypes directly, the interconnectedness of phenotypes should reveal the same picture of temporal scaling of age-related pathologies.

Broader implications of the study

The lifespan of *C. elegans* can be increased by up to 10-fold (Ayyadevara et al., 2008) and decreased by 40-fold, but surprisingly the lifespan curves often follow the same rescaled distribution (Stroustrup et al., 2016). Temporal scaling was also noted when comparing expression profiles of longevity mutants and wild-type *C. elegans* (Tarkhov et al., 2019). Temporal scaling might also be the underlying reason why "aging clocks" based on transcriptional profiling work and longevity mutants' biological age determined by the clock is younger than their chronological age (Meyer and Schumacher, 2021). Furthermore, temporal scaling was also observed for bacterial aging (Yang et al., 2019), suggesting that temporal scaling is an ancient underlying process conserved through evolution. Whether temporal scaling also occurs in mammalian longevity needs to be determined in the future. However, study designs for primary outcome measures for clinical trials on aging are based on the underlying assumption of temporal scaling. For instance, the Metformin in Longevity Study (MILES; NCT02432287) used RNA sequencing of muscle and fat tissue to determine a rejuvenation to a younger expression profile as a primary outcome measure. Interestingly, certain longitudinal *C. elegans* phenotypes are comparable to human age-related phenotypes. Analogous to the *C. elegans* volume increase to peak mid-age and then decrease is that human BMI and waist circumference also follow this early-to-mid-life increase, reaching a peak around 65–70 years and then declining (Kuo et al., 2020). Furthermore, grip strength progressively declines after the age of 30–40 years (Kuo et al., 2020), similar to *C. elegans* muscular strength. This raises the question of whether noncompression of sickspan observed in *C. elegans* means or interpolates to noncompression of sickspan in humans. Because aging is universal, it is tempting to speculate that the underlying mechanisms of aging or age-dependent phenotypes are also universal. This might be a potentially erroneous or unproven extension of the observation that almost all living things age (Freund, 2019). Although phenotypic changes, such as the loss of *C. elegans* muscle force, is analogous to loss of grip strength or muscle strength loss in humans, the underlying biological mechanisms resulting in physical weakness might be different. Our study makes no conclusion or interpolation about the compression of the sickspan in humans.

There is an accumulating body of evidence that long-lived humans are healthy during old age. For instance, 56%–83% and 15%–23% of centenarians, people over the age of hundred years, delay the onset of chronic age-dependent diseases and physical disabilities or were even free of such co-morbidities and frailties, respectively (Ailshire et al., 2015; Evert et al., 2003). Centenarians have lower incidence rates of chronic illnesses compared with their 90- or 80-year-old matched controls (Andersen et al., 2012; Evans et al., 2014; Ismail et al., 2016; Kheirbek et al., 2017). This also extends to family members related to centenarians compared with families without centenarians (Ash et al., 2015; Sebastiani et al., 2013). Thus, centenarians have a later onset and a lower rate of incidence compared with people in their 80s, similar to our observation when comparing longevity mutants with wild-type *C. elegans*. However, because centenarians get to enjoy at least 20 more years, how would this comparison look if we were to compare relative age with chronological age? Is sickspan compressed or temporally scaled in centenarians compared with the average population? As our life expectancy doubled in the last hundred years and we are on the course of potentially reaching the limit of our lifespan (Olshansky and Carnes, 2019), the accompanied delayed onset of disabilities already started to decelerate in longer-lived women compared with men (Freedman et al., 2016). On the other hand, there are several interventions that increase healthspan without increasing lifespan per SE identified in mice (Fischer et al., 2016; Garcia-Valles et al., 2013) and Rhesus monkeys (Mattison et al., 2012). Thus, studying longevity is an important first step of identifying molecular mechanisms promoting healthy aging, but our study and others (Fischer et al., 2016; Garcia-Valles et al., 2013; Mattison et al., 2012) point toward the fact that it is

crucially important for geroscience to start investigating interventions that improve healthspan directly in future studies (Olshansky, 2018). Initial steps in defining healthspan (Kaeberlein, 2017; Kennedy et al., 2014) and also tools and experimental setups, including this study, are being developed to reliably quantify healthspan (Bellantuono et al., 2020; Collins et al., 2008; Haefke and Ewald, 2020; Teuscher et al., 2019; Teuscher and Ewald, 2018).

In summary, we have demonstrated that *C. elegans* sickspan is neither compressed nor extended in longevity mutants, providing an alternative answer to an ongoing debate in the aging field. With our measurements, we showed that previous claims that insulin/IGF-1 receptor mutants have increased sickspan compared with wild type are correct if the voluntary movement is measured but not the case if the muscular function or other healthspan measurements are considered that do not rely on the behavioral state of the animal. By adjusting the reference system from chronological age to relative age, we provide evidence that the healthspan of longevity mutants undergoes temporal scaling. Future studies using our acoustophoresis approach to study the role of healthspan will reveal novel strategies to improve healthy aging.

STAR★METHODS

Detailed methods are provided in the online version of this paper and include the following:

- KEY RESOURCES TABLE
- RESOURCE AVAILABILITY
  - Lead contact
  - Materials availability
  - Data and code availability
- EXPERIMENTAL MODEL AND SUBJECT DETAILS
  - Strains
  - *C. elegans* culturing conditions
- METHOD DETAILS
  - Automated survival assays using the lifespan machine
  - Voluntary movement healthspan measured by lifespan machine
  - Microfluidics device measuring muscle strength
- QUANTIFICATION AND STATISTICAL ANALYSIS
  - Figure generation and statistics

SUPPLEMENTAL INFORMATION

Supplemental information can be found online at https://doi.org/10.1016/j.isci.2022.103983.

AUTHOR CONTRIBUTIONS

All authors participated in analyzing and interpreting the data and designing the experiments. CS performed lifespan assays. PR designed and performed microfluidic assays. CS and PR analyzed the datasets jointly. CS and CYE wrote the manuscript in consultation with the other authors.

DECLARATION OF INTERESTS

The authors have no competing interests to declare.

REFERENCES

Ailshire, J.A., Beltrán-Sánchez, H., and Crimmins, E.M. (2015). Becoming centenarians: disease and functioning trajectories of older US Adults as they survive to 100. J. Gerontol. Ser. A Biol. Sci. Med. Sci. 70, 193–201. https://doi.org/10.1093/gerona/glu124.

Andersen, S.L., Sebastiani, P., Dworkis, D.A., Feldman, L., and Perls, T.T. (2012). Health span approximates life span among many supercentenarians: compression of morbidity at the approximate limit of life span. J. Gerontol. Ser. A Biol. Sci. Med. Sci. 67, 395–405. https://doi.org/10.1093/gerona/glr223.

Ash, A.S., Kroll-Desrosiers, A.R., Hoaglin, D.C., Christensen, K., Fang, H., and Perls, T.T. (2015). Are members of long-lived families healthier than their equally long-lived peers? Evidence from the long life family study. J. Gerontol. Ser. A Biol. Sci. Med. Sci. 70, 971–976. https://doi.org/10.1093/gerona/glv015.

Ayyadevara, S., Alla, R., Thaden, J.J., and Reis, R.J.S. (2008). Remarkable longevity and stress resistance of nematode PI3K-null mutants. Aging Cell 7, 13–22. https://doi.org/10.1111/j.1474-9726.2007.00348.x.

Baasch, T., Reichert, P., Lakämper, S., Vertti-Quintero, N., Hack, G., Solvas, X.C.I., deMello, A., Gunawan, R., and Dual, J. (2018). Acoustic compressibility of Caenorhabditis elegans. Biophysical J. 115, 1817–1825. https://doi.org/10.1016/j.bpj.2018.08.048.

Bansal, A., Zhu, L.J., Yen, K., and Tissenbaum, H.A. (2015). Uncoupling lifespan and healthspan in Caenorhabditis elegans longevity mutants. Proc. Natl. Acad. Sci. 112, E277–E286. https://doi.org/10.1073/pnas.1412192112.

Bellantuono, I., Cabo, R. de, Ehninger, D., Germanio, C.D., Lawrie, A., Miller, J., Mitchell, S.J., Navas-Enamorado, I., Potter, P.K., Tchkonia, T., et al. (2020). A toolbox for the longitudinal assessment of healthspan in aging mice. Nat. Protoc. 15, 540–574. https://doi.org/10.1038/s41596-019-0256-1.

Collins, J.J., Huang, C., Hughes, S., and Kornfeld, K. (2008). The measurement and analysis of age-related changes in Caenorhabditis elegans. WormBook, 1–21. https://doi.org/10.1895/wormbook.1.137.1.

Donnelly, J.L., Clark, C.M., Leifer, A.M., Pirri, J.K., Haburcak, M., Francis, M.M., Samuel, A.D.T., and Alkema, M.J. (2013). Monoaminergic orchestration of motor programs in a complex C. elegans behavior. PLoS Biol. 11, e1001529. https://doi.org/10.1371/journal.pbio.1001529.

Essmann, C.L., Martinez-Martinez, D., Pryor, R., Leung, K.-Y., Krishnan, K.B., Lui, P.P., Greene, N.D.E., Brown, A.E.X., Pawar, V.M., Srinivasan, M.A., and Cabreiro, F. (2020). Mechanical properties measured by atomic force microscopy define health biomarkers in ageing C. elegans. Nat. Commun. 11, 1043. https://doi.org/10.1038/s41467-020-14785-0.

Evans, C.J., Ho, Y., Daveson, B.A., Hall, S., Higginson, I.J., Gao, W., and project, G. (2014). Place and cause of death in centenarians: a population-based observational study in

England, 2001 to 2010. PLoS Med. 11, e1001653. https://doi.org/10.1371/journal.pmed.1001653.

Evert, J., Lawler, E., Bogan, H., and Perls, T. (2003). Morbidity profiles of centenarians: survivors, delayers, and escapers. J. Gerontol. Ser. A 58, 232–237. https://doi.org/10.1093/gerona/58.3.m232.

Ewald, C.Y., Castillo-Quan, J.I., and Blackwell, T.K. (2018). Untangling longevity, dauer, and healthspan in Caenorhabditis elegans insulin/IGF-1-signalling. Gerontology 64, 96–104. https://doi.org/10.1159/000480504.

Ewald, C.Y., Landis, J.N., Abate, J.P., Murphy, C.T., and Blackwell, T.K. (2015). Dauer-independent insulin/IGF-1-signalling implicates collagen remodelling in longevity. Nature 519, 97–101. https://doi.org/10.1038/nature14021.

Ezcurra, M., Benedetto, A., Sornda, T., Gilliat, A.F., Au, C., Zhang, Q., Schelt, S. van, Petrache, A.L., Wang, H., Guardia, Y. de la, et al. (2018). C. elegans eats its own intestine to make yolk leading to multiple senescent pathologies. Curr. Biol. 28, 2544–2556.e5. https://doi.org/10.1016/j.cub.2018.06.035.

Fischer, K.E., Hoffman, J.M., Sloane, L.B., Gelfond, J.A.L., Soto, V.Y., Richardson, A.G., and Austad, S.N. (2016). A cross-sectional study of male and female C57BL/6Nia mice suggests lifespan and healthspan are not necessarily correlated. Aging 8, 2370–2391. https://doi.org/10.18632/aging.101059.

Freedman, V.A., Wolf, D.A., and Spillman, B.C. (2016). Disability-free life expectancy over 30 Years: a growing female disadvantage in the US population. Am. J. Public Health 106, 1079–1085. https://doi.org/10.2105/ajph.2016.303089.

Freund, A. (2019). Untangling aging using dynamic, organism-level phenotypic networks. Cell Syst. 8, 172–181. https://doi.org/10.1016/j.cels.2019.02.005.

Garcia-Valles, R., Gomez-Cabrera, M.C., Rodriguez-Mañas, L., Garcia-Garcia, F.J., Diaz, A., Noguera, I., Olaso-Gonzalez, G., and Viña, J. (2013). Life-long spontaneous exercise does not prolong lifespan but improves health span in mice. Longev. Healthspan. 2, 14. https://doi.org/10.1186/2046-2395-2-14.

Gems, D. (2015). The aging-disease false dichotomy: understanding senescence as pathology. Front. Genet. 6, 212. https://doi.org/10.3389/fgene.2015.00212.

Gems, D., Sutton, A.J., Sundermeyer, M.L., Albert, P.S., King, K.V., Edgley, M.L., Larsen, P.L., and Riddle, D.L. (1998). Two pleiotropic classes of daf-2 mutation affect larval arrest, adult behavior, reproduction and longevity in Caenorhabditis elegans. Genetics 150, 129–155.

Gilpin, W., Uppaluri, S., and Brangwynne, C.P. (2015). Worms under pressure: bulk mechanical properties of C. elegans are independent of the cuticle. Biophys. J. 108, 1887–1898. https://doi.org/10.1016/j.bpj.2015.03.020.

Haefke, A., and Ewald, C. (2020). Tail tendon break time for the assessment of aging and

longitudinal healthspan in mice. Bio-Protocol 10. https://doi.org/10.21769/bioprotoc.3833.

Hahm, J.-H., Kim, S., DiLoreto, R., Shi, C., Lee, S.-J.V., Murphy, C.T., and Nam, H.G. (2015). C. elegans maximum velocity correlates with healthspan and is maintained in worms with an insulin receptor mutation. Nat. Commun. 6, 8919. https://doi.org/10.1038/ncomms9919.

Hess, M., Gomariz, A., Goksel, O., and Ewald, C.Y. (2019). In-vivo quantitative image analysis of age-related morphological changes of C. elegans neurons reveals a correlation between neurite bending and novel neurite outgrowths. eNeuro 6. https://doi.org/10.1523/eneuro.0014-19.2019.

Huang, C., Xiong, C., and Kornfeld, K. (2004). Measurements of age-related changes of physiological processes that predict lifespan of Caenorhabditis elegans. Proc. Natl. Acad. Sci. U S A. 101, 8084–8089. https://doi.org/10.1073/pnas.0400848101.

Hulme, S.E., Shevkoplyas, S.S., McGuigan, A.P., Apfeld, J., Fontana, W., and Whitesides, G.M. (2010). Lifespan-on-a-chip: microfluidic chambers for performing lifelong observation of C. elegans. Lab Chip 10, 589–597. https://doi.org/10.1039/b919265d.

Ismail, K., Nussbaum, L., Sebastiani, P., Andersen, S., Perls, T., Barzilai, N., and Milman, S. (2016). Compression of morbidity is observed across cohorts with exceptional longevity. J. Am. Geriatr. Soc. 64, 1583–1591. https://doi.org/10.1111/jgs.14222.

Kaeberlein, M. (2017). Translational geroscience: a new paradigm for 21st century medicine. Transl. Med. Aging 1, 1–4. https://doi.org/10.1016/j.tma.2017.09.004.

Kennedy, B.K., Berger, S.L., Brunet, A., Campisi, J., Cuervo, A.M., Epel, E.S., Franceschi, C., Lithgow, G.J., Morimoto, R.I., Pessin, J.E., et al. (2014). Geroscience: linking aging to chronic disease. Cell 159, 709–713. https://doi.org/10.1016/j.cell.2014.10.039.

Kenyon, C.J. (2010). The genetics of ageing. Nature 464, 504–512. https://doi.org/10.1038/nature08980.

Kheirbek, R.E., Fokar, A., Shara, N., Bell-Wilson, L.K., Moore, H.J., Olsen, E., Blackman, M.R., and Llorente, M.D. (2017). Characteristics and incidence of chronic illness in community-dwelling predominantly male U.S. Veteran centenarians. J. Am. Geriatr. Soc. 65, 2100–2106. https://doi.org/10.1111/jgs.14900.

Kostka, T. (2005). Quadriceps maximal power and optimal shortening velocity in 335 men aged 23–88 years. Eur. J. Appl. Physiol. 95, 140–145. https://doi.org/10.1007/s00421-005-1390-8.

Kuo, P.L., Schrack, J.A., Shardell, M.D., Levine, M., Moore, A.Z., An, Y., Elango, P., Karikkineth, A., Tanaka, T., Cabo, R. de, et al. (2020). A roadmap to build a phenotypic metric of ageing: insights from the Baltimore Longitudinal Study of Aging. J. Intern. Med. 287, 373–394. https://doi.org/10.1111/joim.13024.

Leong, D.P., Teo, K.K., Rangarajan, S., Lopez-Jaramillo, P., Avezum, A., Orlandini, A., Seron, P., Ahmed, S.H., Rosengren, A., Kelishadi, R., et al. (2015). Prognostic value of grip strength: findings from the Prospective Urban Rural Epidemiology (PURE) study. Lancet *386*, 266–273. https://doi.org/10.1016/s0140-6736(14)62000-6.

López-Otín, C., Blasco, M.A., Partridge, L., Serrano, M., and Kroemer, G. (2013). The hallmarks of aging. Cell *153*, 1194–1217. https://doi.org/10.1016/j.cell.2013.05.039.

Magalhães, J.P. de, Stevens, M., and Thornton, D. (2017). The business of anti-aging science. Trends Biotechnol. *35*, 1062–1073. https://doi.org/10.1016/j.tibtech.2017.07.004.

Mattison, J.A., Roth, G.S., Beasley, T.M., Tilmont, E.M., Handy, A.M., Herbert, R.L., Longo, D.L., Allison, D.B., Young, J.E., Bryant, M., et al. (2012). Impact of caloric restriction on health and survival in rhesus monkeys from the NIA study. Nature *489*, 318–321. https://doi.org/10.1038/nature11432.

Meyer, D.H., and Schumacher, B. (2021). BiT age: a transcriptome-based aging clock near the theoretical limit of accuracy. Aging Cell *20*, e13320. https://doi.org/10.1111/acel.13320.

Olshansky, S.J. (2018). From lifespan to healthspan. J. Am. Med. Assoc. *320*, 1323–1324. https://doi.org/10.1001/jama.2018.12621.

Olshansky, S.J., and Carnes, B.A. (2019). Inconvenient truths about human longevity. J. Gerontol. Ser. A Biol. Sci. Med. Sci. *74*, S7–S12. https://doi.org/10.1093/gerona/glz098.

Partridge, L., Deelen, J., and Slagboom, P.E. (2018). Facing up to the global challenges of ageing. Nature *561*, 45–56. https://doi.org/10.1038/s41586-018-0457-8.

Petrella, J.K., Kim, J., Tuggle, S.C., Hall, S.R., and Bamman, M.M. (2005). Age differences in knee extension power, contractile velocity, and fatigability. J. Appl. Physiol. *98*, 211–220. https://doi.org/10.1152/japplphysiol.00294.2004.

Podshivalova, K., and Kerr, R.A. (2017). How a mutation that slows aging can also disproportionately extend end-of-life decrepitude. Cell Rep. *19*, 441–450. https://doi.org/10.1016/j.celrep.2017.03.062.

Scott, A.J., Ellison, M., and Sinclair, D.A. (2021). The economic value of targeting aging. Nat. Aging, 1–8. https://doi.org/10.1038/s43587-021-00080-0.

Sebastiani, P., Sun, F.X., Andersen, S.L., Lee, J.H., Wojczynski, M.K., Sanders, J.L., Yashin, A., Newman, A.B., and Perls, T.T. (2013). Families enriched for exceptional longevity also have increased health-span: findings from the long life family study. Front. Public Health *1*, 38. https://doi.org/10.3389/fpubh.2013.00038.

Shi, C., and Murphy, C.T. (2014). Mating induces shrinking and death in Caenorhabditis mothers. Science *343*, 536–540. https://doi.org/10.1126/science.1242958.

Stamper, B.L.N., Cypser, J.R., Kechris, K., Kitzenberg, D.A., Tedesco, P.M., and Johnson, T.E. (2018). Movement decline across lifespan of Caenorhabditis elegans mutants in the insulin/insulin-like signaling pathway. Aging Cell *17*, e12704. https://doi.org/10.1111/acel.12704.

Stroustrup, N., Anthony, W.E., Nash, Z.M., Gowda, V., Gomez, A., López-Moyado, I.F., Apfeld, J., and Fontana, W. (2016). The temporal scaling of Caenorhabditis elegans ageing. Nature *530*, 103–107. https://doi.org/10.1038/nature16550.

Stroustrup, N., Ulmschneider, B.E., Nash, Z.M., López-Moyado, I.F., Apfeld, J., and Fontana, W. (2013). The Caenorhabditis elegans lifespan machine. Nat. Methods *10*, 665–670. https://doi.org/10.1038/nmeth.2475.

Tarkhov, A.E., Alla, R., Ayyadevara, S., Pyatnitskiy, M., Menshikov, L.I., Reis, R.J.S., and Fedichev, P.O. (2019). A universal transcriptomic signature of age reveals the temporal scaling of Caenorhabditis elegans aging trajectories. Sci.

Rep. *9*, 7368. https://doi.org/10.1038/s41598-019-43075-z.

Teuscher, A.C., and Ewald, C.Y. (2018). Overcoming autofluorescence to assess GFP expression during normal physiology and aging in Caenorhabditis elegans. Bio-Protocol. *8*. https://doi.org/10.21769/bioprotoc.2940.

Teuscher, A.C., Statzer, C., Pantasis, S., Bordoli, M.R., and Ewald, C.Y. (2019). Assessing collagen deposition during aging in mammalian tissue and in Caenorhabditis elegans. Methods Mol. Biol. Clifton N. J. *1944*, 169–188. https://doi.org/10.1007/978-1-4939-9095-5_13.

United Nations, Department of Economic and Social Affairs, Population Division (2019). World Population Ageing 2019: Highlights*ST/ESA/SER.A/430* (New York: United Nations), pp. 1–46, ISBN: 978-92-1-148325-3.

Yang, Y., Santos, A.L., Xu, L., Lotton, C., Taddei, F., and Lindner, A.B. (2019). Temporal scaling of aging as an adaptive strategy of Escherichia coli. Sci. Adv. *5*, eaaw2069. https://doi.org/10.1126/sciadv.aaw2069.

Zhang, B., Xiao, R., Ronan, E.A., He, Y., Hsu, A.-L., Liu, J., and Xu, X.Z.S. (2015). Environmental temperature differentially modulates C. elegans longevity through a thermosensitive TRP channel. Cell Rep. *11*, 1414–1424. https://doi.org/10.1016/j.celrep.2015.04.066.

Zhang, W.B., Sinha, D.B., Pittman, W.E., Hvatum, E., Stroustrup, N., and Pincus, Z. (2016). Extended twilight among isogenic C. elegans causes a disproportionate scaling between lifespan and health. Cell Syst. *3*, 333–345.e4. https://doi.org/10.1016/j.cels.2016.09.003.

Zhao, Y., Wang, H., Poole, R.J., and Gems, D. (2019). A fln-2 mutation affects lethal pathology and lifespan in C. elegans. Nat. Commun. *10*, 5087. https://doi.org/10.1038/s41467-019-13062-z.

STAR★METHODS

KEY RESOURCES TABLE

REAGENT or RESOURCE	SOURCE	IDENTIFIER
Bacterial and virus strains		
OP50 *Escherichia coli*	https://cgc.umn.edu	OP50-1
L4440 HT115	Ahringer Library	L4440
Biological samples		
C. elegans strain: N2 Bristol (wild type)	https://cgc.umn.edu	N2
C. elegans strain: *eat-2(ad1116)*	https://cgc.umn.edu	DA1116
C. elegans strain: *daf-2(e1370)*	https://cgc.umn.edu	CB1370
C. elegans strain: *daf-2(e1368)*	https://cgc.umn.edu	DR1572
C. elegans strain: *glp-1(e2141)*	https://cgc.umn.edu	CB4037
C. elegans strain: *spe-9(hc88) I; rrf-3(b26) II*	https://cgc.umn.edu	TJ1060
Chemicals, peptides, and recombinant proteins		
5-Fluoro-2′deoxyuridine (FUdR)	Sigma-Aldrich	F0503-1G
Software and algorithms		
lifespan machine code	https://github.com/nstroustrup/lifespan	Flow branch
Other		
Petri dishes with tight-fitting lids	BD Falcon	50 × 9mm
Air-cooled Epson V800 scanners	Epson	V800

RESOURCE AVAILABILITY

Lead contact

Information and requests for resources should be directed to and will be fulfilled by the lead contact: Collin Y. Ewald collin-ewald@ethz.ch.

Materials availability

This study did not generate any new reagents.

Data and code availability

- All data supporting findings of this work are provided within the manuscript and its supplemental information section.
- Microscopy data used in this publication as well as the extracted deviation from the midline can be obtained upon request from the lead contact.

EXPERIMENTAL MODEL AND SUBJECT DETAILS

Strains

Caenorhabditis elegans strains were maintained on NGM plates and OP50 *Escherichia coli* bacteria. The wild-type strain was N2 Bristol. Mutant strains used are described at www.wormbase.org: LGII: *eat-2(ad1116)*; LGIII: *daf-2(e1368, e1370)*, *glp-1(e2141)*.

C. elegans culturing conditions

C. elegans populations were age-synchronized by isolating eggs from gravid *C. elegans* adults, incubating them for 18 hours in M9 until hatching in the presence of 5 μg mL−1 cholesterol (Sigma-Aldrich). Hatched L1-larvae were grown on standard culturing NGM OP50 plates and then shifted to 50 μM FUdR plates

seeded with heat-killed OP50 plates when reaching the L4 state. Animals were maintained on FUdR plates until the measurement of different ages was taken. The *glp-1(e2141)* mutants were placed at 25°C after bleach treatment and shifted back to 15°C at the L4 stage and otherwise treated equally to the other strains. We note that there might be a possible additional lifespan extension from shifting *glp-1* larvae at 25°C during development since wild type N2 grown at 25°C and shifted to 20°C as adults showed increased lifespan (Zhang et al., 2015). Unfortunately, an overall same temperature regime for wild type and all mutants for this study is not possible since *daf-2* mutants would enter into dauer at 25°C during development. Thus, except for *glp-1* during its development, all animals were always maintained and aged at 15°C.

METHOD DETAILS

Automated survival assays using the lifespan machine

To compare the lifespans among wild type and long-lived mutants, we raised all animals for several generations in parallel. Automated survival analysis was conducted using the lifespan machine setup described by (Stroustrup et al., 2013). Briefly, approximately 1000 L4 animals were resuspended in M9 and transferred to NGM plates containing 50 μM 5-Fluoro-2'deoxyuridine (FUdR) seeded with heat-killed OP50 bacteria and incubated at 15°C until day 4 of adulthood. Animals were then resuspended in M9 and transferred to fresh FUdR plates containing tight-fitting lids (BD Falcon Petri Dishes, 50 × 9mm), and the plates were dried with their lids open for 30 minutes after transfer. The plates were incubated for five additional days to rule out contamination and then loaded in the lifespan machine. Air-cooled Epson V800 scanners were utilized for all experiments operating at a scanning frequency of one scan of 30 minutes. Temperature probes (Thermoworks, Utah, US) were used to monitor the temperature on the scanner flatbed and kept constant at 15°C.

For the health-, sick-, life-span validation experiment, we chose to alter three experimental conditions: 1. temperature regime, 2. different bacterial source and live bacteria, and 3. no FUdR. We maintained temperature-sensitive sterile mutants TJ1060 *spe-9(hc88)* I; *rrf-3(b26)* II and *glp-1(e2141)* at 15°C. Synchronized L1 by bleach preparation and let the larvae develop to day-2 adults on OP50 NGM plates at 25°C. Then, we transferred worms onto empty vector L4440 HT115 bacteria at 20°C and at day-8 of adulthood to lifespan plates containing L4440 bacteria to assess lifespan at 20°C.

Voluntary movement healthspan measured by lifespan machine

The time point at which the animal stops moving completely and irretrievably is classified as the point of death and defines the lifespan of each individual. The health- to sickspan transition is estimated by the time point when major movement ceases, and exclusively head movements, posture change, and minor body movements can be observed. The animal is also required to be sedentary and remains in the rough vicinity of the area; it will ultimately die.

Microfluidics device measuring muscle strength

A detailed description of the microfluidics device development and characterization is found in the STAR Methods manuscript https://doi.org/10.2139/ssrn.3890381.

QUANTIFICATION AND STATISTICAL ANALYSIS

Figure generation and statistics

The analysis was performed using the statistical software R. data processing and visualization were performed using the tidyverse package collection, most prominently dplyr and ggplot2. Furthermore, packages were used for lifespan analysis (survival, survminer), computing and visualizing PCA (stats and ggfortify, factoextra), fitting loess models (stats), and segmented fits (segmented), labeling (ggrepel) comparing distributions (ggpubr), and arranging figures (cowplot).